RCS measurements based on a fiber-coupled terahertz time-domain spectrum system

Xu-Tao Zhang(张旭涛), He Cai(蔡禾), Liang-Sheng Li(李粮生), Tao-Ying Yu(庾韬颖), Jin-Fan Liu(刘锦帆), Jin-Hai Sun(孙金海), Zi-Hao Liu(刘子豪), Jin-Chuan Hao(郝津钏)

Citation: Chin. Phys. B. 35, 104101 (2026). DOI: 10.1088/1674-1056/ae29f8 | CSTR: 32038.14.CPB.ae29f8
http://cpb.iphy.ac.cn; http://iopscience.iop.org/cpb

What follows is a list of articles you may be interested in

Detection and identification of three types of kaolin using terahertz time-domain spectroscopy

Qi Sun(孙齐), Shuguang Miao(苗曙光), Qiuyue Zhang(张秋悦), Shuangwu Shi(施双伍), Xiaonuo Hou(侯晓诺)

Chin. Phys. B. 35, 094101 (2026). DOI: 10.1088/1674-1056/ae1c1d | CSTR: 32038.14.CPB.ae1c1d

Compact multimode vortex-wave radiator enabled by quasi-1D spoof plasmons

Zhen Liao(廖臻), Zuquan Ao(敖祖权), Yun Li(李赟), Guo-Qing Luo(罗国清), Leilei Liu(刘蕾蕾)

Chin. Phys. B. 35, 084101 (2026). DOI: 10.1088/1674-1056/ae5f85 | CSTR: 32038.14.CPB.ae5f85

Tunable terahertz transmission behaviors and coupling mechanism in hybrid MoS_2 metamaterials

Yuwang Deng(邓雨旺), Qingli Zhou(周庆莉), Wanlin Liang(梁菀琳), Pujing Zhang(张朴婧), Cunlin Zhang(张存林)

Chin. Phys. B. 31, 014101 (2022). DOI: 10.1088/1674-1056/ac1fde

Terahertz radiation generation by beating of two chirped laser pulses in a warm collisional magnetized plasma

Motahareh Arefnia, Mehdi Sharifian, Mohammad Ghorbanalilu

Chin. Phys. B. 30, 094101 (2021). DOI: 10.1088/1674-1056/abfb5d

Surface plasmon polaritons frequency-blue shift in low confinement factor excitation region

Ling-Xi Hu(胡灵犀), Zhi-Qiang He(何志强), Min Hu(胡旻), Sheng-Gang Liu(刘盛纲)

Chin. Phys. B. 30, 084102 (2021). DOI: 10.1088/1674-1056/abe22e

---

RCS measurements based on a fiber-coupled terahertz time-domain spectrum system

Xu-Tao Zhang(张旭涛)†, He Cai(蔡禾), Liang-Sheng Li(李粮生), Tao-Ying Yu(庾韬颖), Jin-Fan Liu(刘锦帆), Jin-Hai Sun(孙金海), Zi-Hao Liu(刘子豪), and Jin-Chuan Hao(郝津钏)

National Key Laboratory of Scattering and Radiation, Beijing 100143, *China*

(Received 30 March 2025; revised manuscript received 13 November 2025; accepted manuscript online 9 December 2025)

Current terahertz devices exhibit low radiation power, and terahertz target scattering characterization measurements are predominantly conducted in indoor environments. Terahertz time-domain spectroscopy (THz-TDS) systems, with their broadband, high sensitivity, and quasi-optical characteristics, are particularly suitable for compact-range scale-model and small-target measuring in indoor environments. By leveraging a fiber-optic coupled transceiver link and compact-range design, a TDS scattering characterization measurement system with a total transmission path exceeding 20 m was implemented in an anechoic chamber. This system successfully measured the high-accuracy radar cross section (RCS) of targets with larger size within the 0.3–2 THz. The RCS of a metallic scale model was measured and compared with simulation results from rapid computational methods to validate applicability. Furthermore, high-frequency scattering theoretical calculation methods for large-scale targets in the terahertz band and the application scenarios of scale-model measurements were explored.

Keywords: terahertz, time-domain spectrum, radar cross section

PACS: 41.20.Jb, 42.25.Fx, 84.40.–x, 87.50.U

DOI: 10.1088/1674-1056/ae29f8 **CSTR:** 32038.14.CPB.ae29f8

1. Introduction

Terahertz waves (0.1–10 THz), characterized by their broad bandwidth, high resolution, and strong penetration capabilities, hold immense potential for applications in radar target detection, stealth technology, object identification, and non-destructive testing. However, practical implementation has been constrained by technological limitations in device development and signal attenuation in atmospheric conditions. Current radar target measurement systems are predominantly confined to indoor environments, which primarily employ two types of setups. The first category involves microwave frequency multiplication systems operating within atmospheric transmission windows at lower THz frequencies (e.g., 220 GHz and 340 GHz). These systems feature compact hardware designs and can achieve Watt-level radiation power, making them highly practical. Notably, in 1991, McMillan's research team at the Georgia Institute of Technology pioneered the development of a 225 GHz pulsed coherent experimental radar system, marking a significant milestone in THz radar technology.[1] In 2008, the Jet Propulsion Laboratory (JPL) in California, USA developed a radar system with a center frequency of 580 GHz for imaging and measurement purposes.[2] After that, the JPL developed a 675 GHz radar system, achieving a dramatic enhancement in imaging speed in 2011.[3] The Submillimeter-wave Technology Laboratory at the University of Massachusetts Lowell has established multiple compact range measurement systems operating at 160 GHz, 240 GHz and 524 GHz. Based on these systems, they have conducted in-depth research on target scattering characteristics.[4–7] The German Research Center for High-Frequency Physics and Radar Technology successfully developed the Miranda-300 radar, operating at a frequency of 0.3 THz. This radar achieved inverse synthetic aperture radar (ISAR) imaging of concealed targets at a distance of 700 m, with a resolution of 3.75 mm.[8]

The National University of Defense Technology (NUDT) has established indoor measurement systems operating at 220 GHz, 330 GHz, and 440 GHz to conduct RCS measurements and imaging on multiple types of targets.[9,10] In 2011, the China Academy of Engineering Physics (CAEP) constructed the nation's first 140 GHz high-resolution ISAR imaging experimental system using self-developed terahertz devices.[11] In 2013, CAEP further achieved a breakthrough by completing a 670 GHz all-solid-state imaging radar system.[12]

The second category is the optical down-conversion system:[13,14] there are mainly the terahertz time-domain spectrum system and terahertz lasers. The time-domain spectrum system uses ultrashort laser pulses to excite broadband terahertz waves, which enables the miniaturization of the equipment. It covers frequencies from 0.1 THz to 5 THz or even higher. However, its radiation power is the lowest, on the order of milliwatts, but it can detect weak time-domain signals. Transmission loss through water vapour is significant.

†Corresponding author. E-mail: mi_zhangxt@163.com

© 2026 Chinese Physical Society and IOP Publishing Ltd. All rights, including for text and data mining, AI training, and similar technologies, are reserved.

In 2010, the Technical University of Denmark obtained the omnidirectional RCS measurement results of a 1:150 scale F-16 fighter model at frequency points of 0.3 THz, 0.7 THz, and 1.1 THz based on the time-domain spectrum measurement system, and conducted an imaging test on the scale model.[15] In 2012, the University of Marburg in Germany conducted experimental measurements on the terahertz scattering characteristics of standard objects and scaled-down aircraft models.[16] Tianjin University conducted RCS measurements on scale models of tanks and aircraft carriers using a THz-TDS system in 2014, achieving two-dimensional scattering imaging of the targets.[17] In 2016, Huazhong University of Science and Technology conducted experimental measurements on the terahertz scattering characteristics of metal plates using a THz-TDS system with an output frequency range of 0.2–2 THz.[18] In 2022, Menlo Systems and the Fraunhofer Heinrich Hertz Institute (HHI) reported the collaborative development of an all-fiber-coupled THz-TDS system. Under a laser excitation power of 55 mW, the system generated terahertz waves with 0.97 mW output power, achieving a bandwidth of 6.5 THz and a peak dynamic range of 101 dB.[19] Terahertz lasers utilize high-power laser excitation of gases to generate intense terahertz waves at specific spectral lines (e.g., 1.56 THz, 2.4 THz, and 2.52 THz).[20–23] These systems are typically characterized by larger equipment sizes, with terahertz wave radiation power often reaching hundreds of milliwatts. In 2015, the University of Queensland in Australia established a 2.59 THz test system to study the backscattering characteristics of metallic cubes in the terahertz regime.[24] Harbin Institute of Technology developed a 2.52 THz test system that achieved transmission imaging of occluded objects.[25,26] Tianjin University further conducted RCS measurements on targets using the 2.52 THz measurement system.[27]

Microwave frequency multiplier systems of terahertz demonstrate significant practical value in modern defense and detection fields due to their compact size, high power output (Watt-level power @220 GHz), weaker atmospheric attenuation, and mature technological readiness. These systems excel in applications like precision guidance and stealth detection.

2. System and measurements

The terahertz time-domain spectroscopy system comprises transmitter, transmission, receiver, and data acquisition modules. Specifically, the transmitter employs a femtosecond laser-pumped THz photoconductive antenna (e.g., GaAs-based) to generate broadband THz waves through transient current radiation under bias voltage; the transmission path utilizes off-axis parabolic mirrors for collimation and nitrogen-purged environments to minimize atmospheric absorption (shown in Fig. 1). In the receiver, the inverse process occurs: the THz wave is captured by a photoconductive sampling antenna, where femtosecond laser-induced carriers are modulated by the THz field to generate nanoampere-level currents. These weak signals undergo amplification via a current preamplifier, followed by noise suppression and phase-sensitive extraction using a lock-in amplifier synchronized with the laser repetition frequency. Finally, the processed signals are digitized for spectral analysis through Fourier transform.

The system adopts a fiber-coupled femtosecond laser (pre-dispersion compensated to achieve $>$ 100 fs pulse width at the antenna) for both THz generation and detection. To broaden the THz spectral bandwidth in compact field measurements, a 3 ns delay line is integrated to accommodate target dimensions. Polarization control is implemented via in-line polarizers to mitigate polarization extinction ratio degradation caused by differential group delay in fiber components, which otherwise induces dual-signal artifacts from elliptical polarization conversion. The free-space propagation path (exceeding 20 m for wide beam coverage) is housed in an anechoic chamber with active temperature/humidity control ($<$ 10% RH during operation) to minimize atmospheric absorption loss. Testing shows that the peak-to-peak signal amplitude of this system at 4% humidity is 1.6 times that at 10% humidity. The optical alignment employs off-axis parabolic mirrors with sub-wavelength positioning accuracy, synchronized with motorized stages for dynamic beam steering.

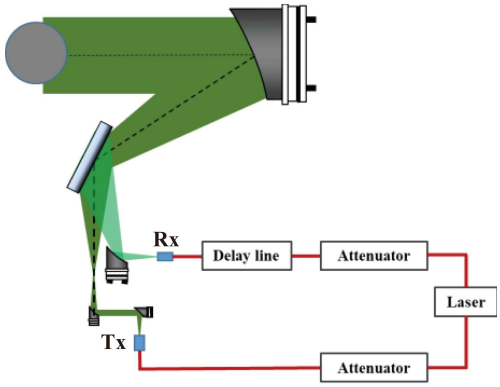

Fig. 1. Schematic diagram of system settings.

The laser pulses in both the transmitter path and the detection path have successfully achieved the designed narrow pulse width (measured by an autocorrelator to be $<$ 100 fs, as shown below), which ensures optimal broadband THz wave generation from the photoconductive antenna.

The system employs a high-speed delay line to achieve rapid scanning while maintaining repeated positioning accuracy. This enables multi-cycle acquisition of raw time-domain signals within the allocated time. Through arithmetic averaging of these datasets, the signal-to-noise ratio (SNR) is effectively enhanced — the SNR improvement scales with the accumulated signal repetitions. Experimental results demonstrate a minimum 20 dB SNR compared to single-shot measurements.

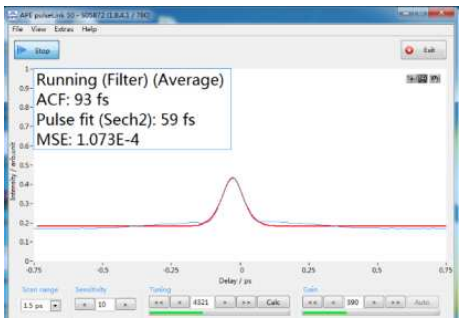

Fig. 2. Measured results of laser pulse width in the transmission path (with the transmitting antenna replaced by equal-length optical fiber).

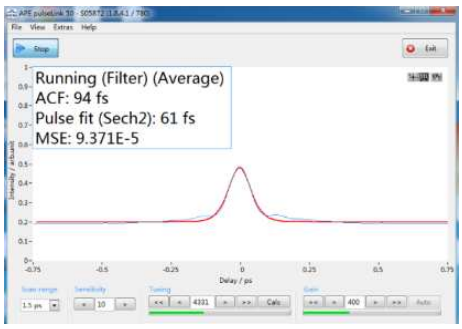

Fig. 3. Measured results of laser pulse width in the detection path (with the receiving antenna replaced by equal-length optical fiber).

Fig. 4. Terahertz time-domain spectroscopy compact range.

The measurement results of the metallic cube demonstrate an RCS spanning 0.3–2 THz, with all errors maintained within ± 1.5 dB, thereby validating the system's RCS measurement capability in the terahertz band. In this system, the main uncertainty components considered include near-field, drift, noise-background and reference RCS. Therefore, the measurement uncertainty is about ± 2 dB.

The extensive deployment of small drones in the Russia–Ukraine conflict has underscored their growing military significance, necessitating global efforts to develop countermeasures. Terahertz radar, with its sub-millimeter wavelength resolution, provides an effective solution by enabling high-precision detection of low-observable targets. Initial trials have successfully captured the scattering characteristics of small drones.

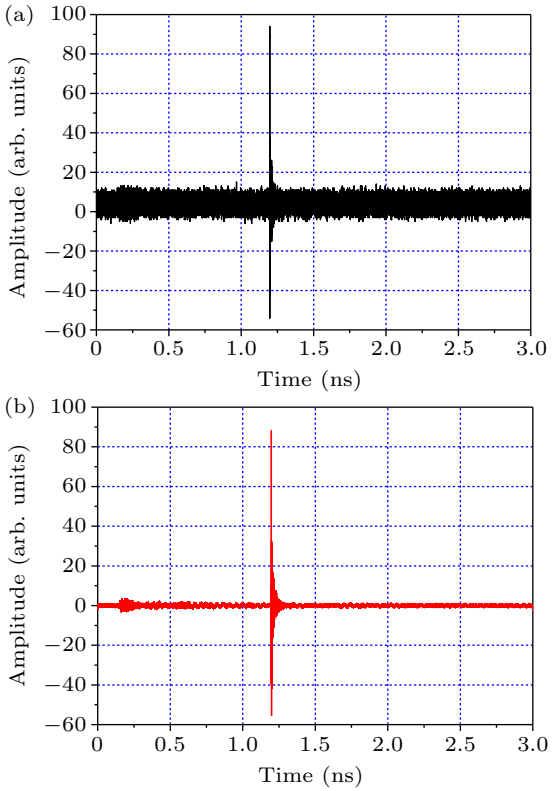

Fig. 5. Comparison of signals before and after data processing: (a) raw acquired signal, (b) time-domain averaged and filtered signal.

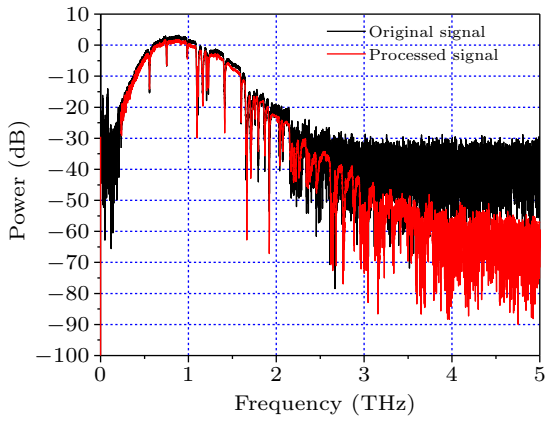

Fig. 6. Comparison of frequency domain characteristics before and after signal data processing.

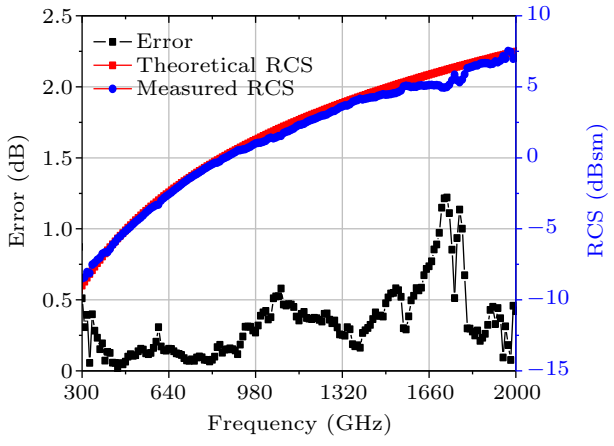

Fig. 7. RCS measurement results of a metal cube with edge length 10 mm.

This paper conducts experimental measurements on a small unmanned aerial vehicle (UAV), and its 1D high-resolution range profile (HRRP) is shown in the figure below. Two dominant scattering peaks are observed in the HRRP: peak 1 originates from the camera module, while peak 2 corresponds to the battery pack. Most UAV rotor wings (mainly plastic materials) exhibit weak scattering characteristics with some terahertz wave absorption. The compact design of miniature rotor motors also results in few radar returns. After calibration processing, the UAV's terahertz-band RCS magnitude measures approximately −20 dBsm.

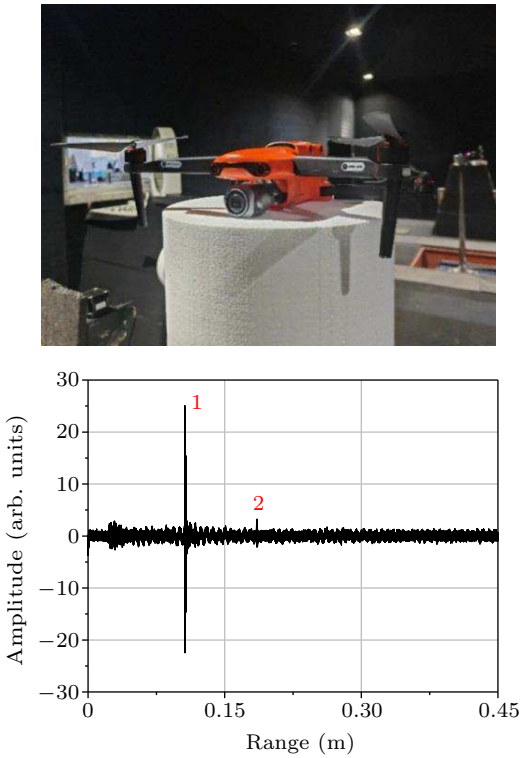

Fig. 8. Measurement results of 1D HRRP for the AUTEL EVOII UAV.

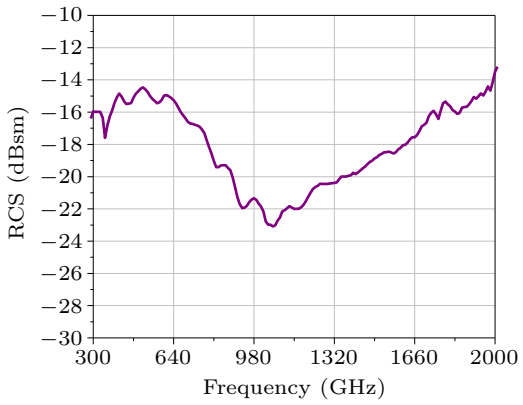

Fig. 9. RCS measurement results of the AUTEL EVOII UAV.

Compared to free-space TDS, fiber-based TDS offers more convenient system deployment and higher integration. However, TDS RCS measurement systems are typically limited to small-size targets, which severely restricts their applicability. The system developed in this work successfully acquired measurements for larger-sized miniature unmanned aerial vehicles, greatly expanding the range of measurable targets. Furthermore, compared to microwave frequency-multiplier systems, TDS provides extremely high spatial resolution and ultra-wide bandwidth. The spatial resolution along the longitudinal direction in microwave frequency-multiplier systems primarily depends on their bandwidth, which is significantly narrower than that of TDS.

3. Scale model RCS simulation and measurement

Due to the prevalence of electrically large targets in the terahertz band, numerical simulation algorithms face an extremely high computational load, making it challenging to model real-world targets and scenarios.[28–30] This study employs a high-frequency asymptotic theory-based fast algorithm for simulation and validates its accuracy through measurement, laying the foundation for further improvements and applications of such algorithms in the terahertz band.

3.1. Theoretical calculation

Electromagnetic scaling relationships for perfect electric conductor (PEC) targets are given as follows.[31]

When the RCS of a $1:s$ scale model (σ') has the following relationship with the RCS scaled to the full-size (1:1) target (σ):

$$\sigma = \sigma' + 20\lg s\ (\mathrm{dB}).$$

Correspondingly, the measuring frequency f' of the scale model should be s times that of the actual target's measuring frequency f.

According to the scaling law, a full-scale perfect electrical conductor (PEC) model with a base diameter of 0.5 m and a height of 1.78 m is shown in Fig. 10. The target is scaled down at a 1:16.67 ratio, resulting in a metal scale model with a height of 106.80 mm and a base diameter of 30 mm. The RCS calculation frequency for the full-scale model is set at 30 GHz, while the measurement frequency for the scale model is set at 500 GHz. Consequently, the full-scale model constitutes an electrically large target, necessitating the use of high-frequency modeling methods for RCS computation.

Electromagnetic scattering modeling for high-frequency band targets primarily employs high-frequency asymptotic theory-based computational methods to analyze complex target scattering characteristics.[31–36] This study adopts a facet-based geometric model, utilizing the physical optics (PO) method and the equivalent edge current (EEC) method to calculate the contributions of primary reflections and edge diffraction from complex targets, while employing the ray tracing (RT) technique to account for multiple reflection contributions.

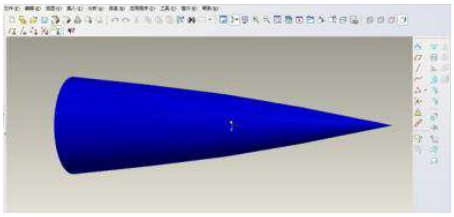

Fig. 10. Simulating full-scale model.

High-frequency scattering primarily comprises five scattering mechanisms, whose combinations form the RCS characteristics of complex targets. These mechanisms include: (1) specular reflection; (2) scattering from surface discontinuities (e.g., edges, corners, and tips); (3) scattering due to surface derivative discontinuities (e.g., curvature breaks); (4) scattering from concave regions (e.g., cavities, dihedrals, and trihedrals); (5) interaction scattering (e.g., multipath scattering or multiple interactions between scattering centers).

High-frequency scattering is closely related to the local structure of targets. Different scattering mechanisms often require distinct high-frequency analysis methods. Among these mechanisms, specular reflection is a strong scattering mechanism, typically analyzed using geometric optics or physical optics. Edge discontinuities and surface irregularities exhibit diffraction phenomena, which represent another significant scattering mechanism usually addressed through geometric diffraction theory or equivalent electromagnetic current methods. Scattering from concave regions often produces strong echoes across a wide angular domain, but its complex process poses challenges for conventional theoretical methods. This paper employs an improved ray-tracing technique to calculate multiple reflection contributions. For complex targets, accounting for these dominant mechanisms generally yields satisfactory results. Additionally, incorporating scattering contributions from special structures (slots, tips, etc.) can significantly enhance electromagnetic scattering calculation accuracy. Under high-frequency conditions, electromagnetic wave reflection follows the geometric optics reflection law.

Based on the aforementioned theoretical methods, the calculated full-azimuth RCS results of the full-scale model at 30 GHz are shown in Fig. 11.

As shown in Fig. 11, near 0°, the primary scattering mechanism originates from the tip scattering of the model. Near 90°, it is dominated by strong specular reflection from the side surfaces of the model. Near 180°, the main contribution arises from strong specular scattering at the base surface of the model.

Simultaneously, the omnidirectional RCS of the 500 GHz scale model was calculated using the same method, demonstrating strong consistency with the computational results of the 30 GHz full-scale model.

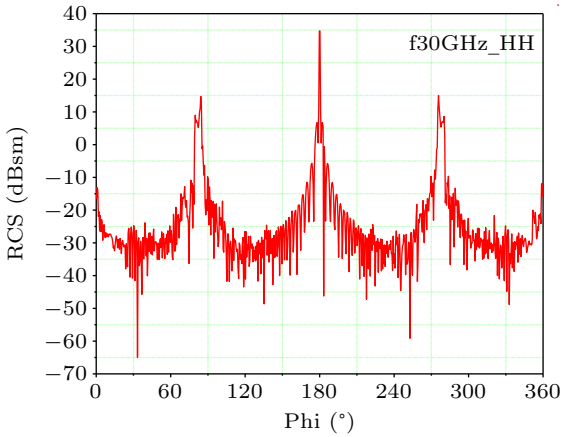

Fig. 11. Simulation RCS of full-scale model.

3.2. Measurement results

As shown in Fig. 12, the scale model has a surface roughness of less than 3 micrometers. Based on calibration measurements, multi-angle echo measurements and RCS calibration were conducted for the metallic scale model.

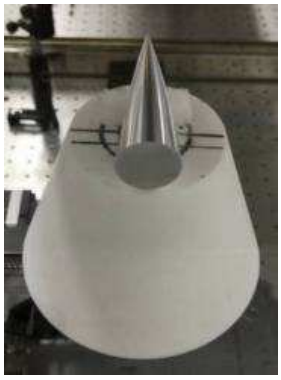

Fig. 12. Measuring scale model.

During the measurement process, to ensure the accuracy of the azimuth angle, the model orientation at 180° is first determined by adjusting the base disk of the model to face the transmit–receive waves directly. Near the estimated 180° position, echoes are measured at different azimuth and elevation angles. The azimuth angle corresponding to the maximum echo intensity is identified as the true 180° reference. Using this angle as the benchmark, the model echoes are then measured across varying azimuth angles.

The azimuthal RCS of the measured scale model is shown in Fig. 13. RCS values at certain angles were not acquired due to excessively low RCS values, where time-domain echoes were too weak or submerged in noise, making extraction impossible and resulting in invalid RCS data. For the measured angular RCS results, the maximum deviation does not exceed 3 dB compared to theoretical values. The symmetrical 0°–360° RCS results are shown in Fig. 14.

When the model's top faces the incoming wave direction, extremely weak scattering mechanisms such as tip scattering, edge scattering, creeping waves, and traveling waves

are observed. Unlike the microwave band, terahertz waves exhibit exceptional directionality, causing most incident energy to undergo forward scattering upon interacting with the target. Consequently, minimal scattered energy returns to the receiving parabolic mirror, resulting in undetectable signals. For the same reason, no effective echo signals can be measured within a certain angular range near 0°.

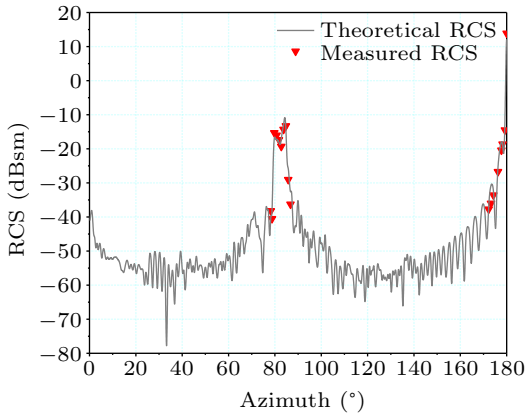

Fig. 13. Scale model RCS measurements and simulation results of 0°–180°.

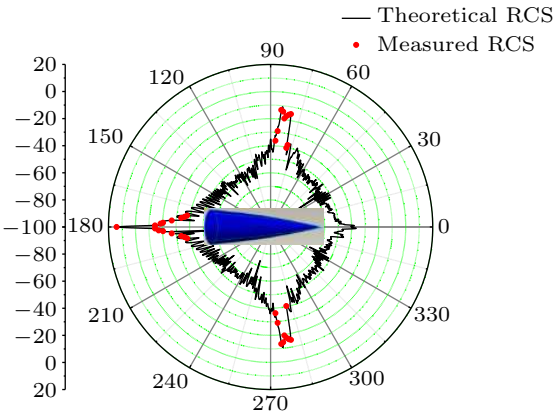

Fig. 14. Scale model RCS measurement and simulation results of 0°–360°.

4. Conclusion and perspectives

A laser-based all-fiber THz-TDS RCS measurement system was established. In an anechoic chamber environment, despite the free-space optical path of the terahertz wave exceeding 20 m, broadband and high dynamic-range echo signals were still acquired. Validated by calibration targets, the measurement error remained within ±1.5 dB. Subsequently, the scattering characteristics of small unmanned aerial vehicles were tested, providing critical support for potential applications of terahertz radar in counter-small UAV scenarios.

Using a high-frequency fast method, the 0°–360° azimuthal RCS of both the 30 GHz full-scale metallic model and the 500 GHz scale model was simulated. The RCS of the metallic scale model was subsequently measured using a terahertz TDS target scattering characterization system. Based on the electromagnetic scaling theory for perfect electric conductor targets, the computational and experimental results were compared, showing errors within 3 dB. This validates the feasibility of high-frequency theoretical fast computation methods for electrically large-scale targets in the terahertz band. When calculating the RCS of a full-scale model using high-frequency methods, all scattering mechanisms are comprehensively accounted for, with distinct theoretical approaches applied to different mechanisms. However, during experimental measurements of the scale model's RCS, weak scattering mechanisms such as creeping waves and tip scattering often remain undetectable due to noise interference in echo signals, leading to discrepancies between theoretical predictions and measured values.

References

[1] McMillan R W, Trussell C W, Bohlander R A, Butterworth J and Forsythe R E 1991 *IEEE Trans. Microwave Theory Tech.* **39** 555

[2] Cooper K B, Dengler R J, Chattopadhyay G, Schlecht E, Gill J and Skalare A 2008 *IEEE Microw. Wireless Compon. Lett.* **18** 64

[3] Cooper K B, Dengler R J, Llombart N, Thomas B, Chattopadhyay G and Siegel P H 2011 *IEEE Trans. Terahertz Sci. Technol.* **1** 169

[4] DeMartinis G B, Coulombe M J, Horgan T M, Giles R H and Nixon W E 2010 *Proceedings of AMTA* p. 3

[5] Goyette T M, Dickinson J C, Gorveatt W J, Waldman J and Nixon W E 2004 *Proc. SPIE* **5427** 227

[6] Coulombe M J, Horgan T, Waldman J, Szatkowski G and Nixon W E 1999 *Proceedings of AMTA* p. 458

[7] Coulombe M J, Ferdinand T, Horgan T, Giles R and Waldman J 1993 *Proceedings of AMTA* p. 129

[8] Stanko S, Palm S, Sommer R, Kloppel F, Caris M and Pohl N 2016 *Proceedings of the 2016 46th European Microwave Conference*, October 4–6, 2016, London, England 1505–1508

[9] Song Y, Li Y P, Pang S, Zhao S S and Wang H Q 2018 *Electron. Lett.* **54** 714

[10] Wang R J 2015 *Research on Key Technology of Target Scattering Characteristics at Terahertz Frequencies* (Ph.D. Dissertation) (Changsha: National University of Defense Technology) (in Chinese)

[11] Cheng B B, Jiang G, Wang C and Yang C 2013 *IEEE Trans. Terahertz Sci. Technol.* **3** 594

[12] Cheng B B, Jiang K, Chen P, Yang C, Lu B, Cai Y W, Deng X J, Chen Z, Zhang J and Zhou C M 2013 *J. Terahertz Sci. Electron. Inf. Technol.* **11** 7

[13] Ding J, Meng Q H, Shen Y, Ding C X, Su B, Cui H L and Zhang C L 2023 *Chin. Phys. B* **32** 742

[14] Wang R J, He S and Zhang H 2024 *IEEE 7th International Conference on Electronic Information and Communication Technology (ICEICT)* (Xi'an, China) p. 124

[15] Iwaszczuk K, Heiselberg H and Jepsen P U 2010 *Opt. Express* **18** 26399

[16] Gente R, Jansen C, Geise R, Peters O, Gente M, Krumbholz N, Moller C, Busch S F and Koch M 2012 *IEEE Trans. Terahertz Sci. Technol.* **2** 424

[17] Liang D C, Wei M G and Gu J Q 2014 *Acta Phys. Sin.* **63** 214102 (in Chinese)

[18] Nie X Y, Xiang F D, Huang X, Liu J S, Yang Z G and Wang K J 2016 *Laser Technol.* **40** 676

[19] Kohlhaas R, Gingras L, Dardanis E, Holzwarth R, Breuer S, Schell M and Globisch B 2022 *47th IRMMW-THz* (Delft, Netherlands) p. 1

[20] Goyette T M, Dickinson J C, Waldman J and Nixon W E 2000 *Proc. SPIE* **4053** 615

[21] Goyette T M, Dickinson J C, Linden K J, Neal W R, Joseph C S, Gorveatt W J, Waldman J, Giles R and Nixon W E 2008 *Conference on Terahertz Technology and Applications* (San Jose, US) p. 23

[22] Goyette T M, Dickinson J C, Waldman J, Nixon W E and Carter S 2001 *Proc. SPIE* **4382** 229

[23] Danylov A A, Goyette T M, Waldman J, *et al.* 2010 *Opt. Express* **18** 16264

[24] Lui H S, Taimre T, Bertling K, Lim Y L, Davies A G and Rakic A D 2015 *Electron. Lett.* **51** 1774

[25] Li Q, Yao R, Ding S H and Wang Q 2011 *Chin. J. Lasers* **38** 0711001

[26] Cheng K Y and Li Q 2021 *Chin. J. Lasers* **48** 195

[27] Qiao H Z, Zhong K, Shi J, Liu Y, Liu K F, Xu D G and Yao J Q 2021 *J. Infrared Millim. Waves* **40** 341

[28] Ang Y X and Lui H S 2023 *Sensors* 23 7202

[29] Pang S, Zeng Y and Deng Y B 2024 *IEEE Trans. Antennas Propag.* **72** 1850

[30] Pang S, Zeng Y and Yang Q 2022 *Chin. Phys. B* **31** 068703

[31] Huang P K, Yin H C, Xu X J and Bai Y 2005 *Radar Target Characteristics* (Beijing: Publishing House of Electronics Industry) p. 21 (in Chinese)

[32] Chen H, Xu L, Zhang Y and Cui T J 2018 *J. Radars* **7** 108

[33] Syed H H and Volakis J 1996 *IEEE Trans. Antennas Propag.* **44** 983

[34] Shore R A and Yaghjian A D 2001 *IEEE Trans. Antennas Propag.* **49** 200

[35] Yaghjian A D, Shore R A and Woodworth M B 1996 *Radio Sci.* **31** 1681

[36] Michaeli A 1986 *IEEE Trans. Antennas Propag.* **34** 912